



HAL
open science

Vibrational dynamics of confined supercooled water

E. Stefanutti, L. Bove, Frederico Alabarse, G. Lelong, F. Bruni, M. A Ricci

► **To cite this version:**

E. Stefanutti, L. Bove, Frederico Alabarse, G. Lelong, F. Bruni, et al.. Vibrational dynamics of confined supercooled water. *Journal of Chemical Physics*, 2019, 150 (22), pp.224504. 10.1063/1.5094147 . hal-02173067

HAL Id: hal-02173067

<https://hal.sorbonne-universite.fr/hal-02173067>

Submitted on 8 Jun 2022

HAL is a multi-disciplinary open access archive for the deposit and dissemination of scientific research documents, whether they are published or not. The documents may come from teaching and research institutions in France or abroad, or from public or private research centers.

L'archive ouverte pluridisciplinaire **HAL**, est destinée au dépôt et à la diffusion de documents scientifiques de niveau recherche, publiés ou non, émanant des établissements d'enseignement et de recherche français ou étrangers, des laboratoires publics ou privés.



Distributed under a Creative Commons Attribution - NonCommercial 4.0 International License

Vibrational dynamics of confined supercooled water

E. Stefanutti,^{1,2}  L. E. Bove,^{1,a)}  F. G. Alabarse,^{1,b)}  G. Lelong,¹  F. Bruni,²  and M. A. Ricci^{2,c)} 

¹Sorbonne Université, Muséum National d'Histoire Naturelle, UMR CNRS 7590, IRD, Institut de Minéralogie, de Physique des Matériaux et de Cosmochimie, IMPMC, 4 Place Jussieu, 75005 Paris, France

²Dipartimento di Scienze, Università Degli Studi Roma Tre, Via della Vasca Navale 84, 00146 Roma, Italy

^{a)}**Present address:** Dipartimento di Fisica, Sapienza Università Degli Studi di Roma, Piazzale A. Moro 2, 00185 Roma, Italy.

^{b)}**Present address:** Elettra Sincrotrone Trieste, Area Science Park, 34149 Basovizza TS, Italy.

^{c)}mariaantonia.ricci@uniroma3.it

The quest for a possible liquid-liquid coexistence line in supercooled water below its homogeneous nucleation temperature is faced by confining water within a porous silica substrate (MCM-41). This system is investigated by synchrotron radiation infrared spectroscopy, exploring both the intramolecular and the intermolecular vibrational dynamics, in the temperature range from ambient down to ~ 120 K, along several isobaric paths between 0.7 kbar and 3.0 kbar. Upon lowering the temperature, the OH-stretching band shows that the intramolecular vibrational dynamics continuously evolves from predominantly liquidlike to predominantly icelike. An abrupt change in the line shape of the intermolecular vibrational band between 220 K and 240 K, depending on the pressure, is the signature of nucleation of ice within the MCM-41 pores. These findings do not support the presence of two liquid phases and provide evidence for the coexistence of liquid water and ice in water confined in MCM-41.

I. INTRODUCTION

In many situations relevant to our life and environment, water is confined in small volumes or at the surface of a substrate. This is, for instance, the case of water within rocks and minerals or in living cells, and many other examples can be made, encompassing fields such as geology, biology, and technological applications. Consequently, it is not surprising that rich literature on confined water has been published (see, for instance, Refs. 1–3 and references therein) since the seminal work of Hawkins and Egelstaff in 1980.⁴ This literature shows that a few features common to all instances of confined water can be identified although structural and dynamical details may depend on the properties of the confining substrate, such as hydrophilicity,⁵ chemical heterogeneity,⁶ and topography.⁷ In particular, both experiments and simulations establish that at the substrate surface, there is a layer of water molecules with a higher density and a slower dynamics^{3,5,6,8–13} compared to molecules distant from it (for instance, in the middle of a pore). Both these

observations suggest that a direct comparison between bulk and confined water requires caution although the two share some common features, as, for instance, a line of maximum density or the purported fragile to strong crossover, FSC.³

It is well known that confinement allows us to decrease the melting temperature of water well below the homogeneous nucleation temperature, $T_H \sim 232$ K, as it reduces the extension of the hydrogen bonded (HB) network^{14,15} while preserving the key tetrahedral local geometry. This is one of the reasons why some organisms can survive at low temperatures and liquid micrometer droplets occur in cirrus clouds. The possibility to shift the melting temperature below T_H has paved the way to a lively research aimed at understanding the known water anomalies by experiments performed on confined water at low temperatures.

As a matter of fact, several properties of water such as density, thermal expansion coefficient, isothermal compressibility, and isobaric heat capacity have an anomalous absolute value and temperature dependence at low temperatures, in the supercooled metastable

state, between $T_M = 273$ K and T_H .¹⁷ Several conjectures have been proposed to explain these anomalies, the most popular being the retracing spinodal,¹⁸ the singularity free scenario,¹⁹ and the second critical point hypothesis.²⁰ The key for discriminating among these conjectures resides in the ability of probing water properties in a low temperature thermodynamic range that is experimentally not accessible in bulk water. This thermodynamic range, named *No man's land* (see Fig. 1),¹⁷ has instead been thoroughly investigated by Molecular Dynamics (MD) simulations^{19–25} because ice nucleation can in principle be controlled in silica. As a result of a controversial debate, it has been established that MD simulations report unambiguous signatures of distinct liquid-liquid, L - L , and liquid-crystal, L - X , transitions in several models of bulk supercooled water.²⁵

Given the relevance and fascination of the second critical point scenario, the experimental research has used tricks in order to enter the *No man's land*, the most popular being confinement in the small volumes of micelles and microemulsions,¹⁷ porous silica glasses,^{3,8–11,26,27} or droplets.²⁸ Exhaustive account of all literature concerning this experimental quest for a second critical point and a liquid-liquid transition under confinement is unfeasible here; nevertheless, we mention that clear, convincing experimental evidence has not yet been achieved.^{29–34}

Here, we use synchrotron radiation infrared (IR) spectroscopy to investigate the vibrational dynamics of water confined in a porous silica matrix, over a wide temperature and pressure range, along the isobaric lines shown in Fig. 1 as blue arrows. IR spectroscopy is an ideal technique which can be exploited to probe even small amounts

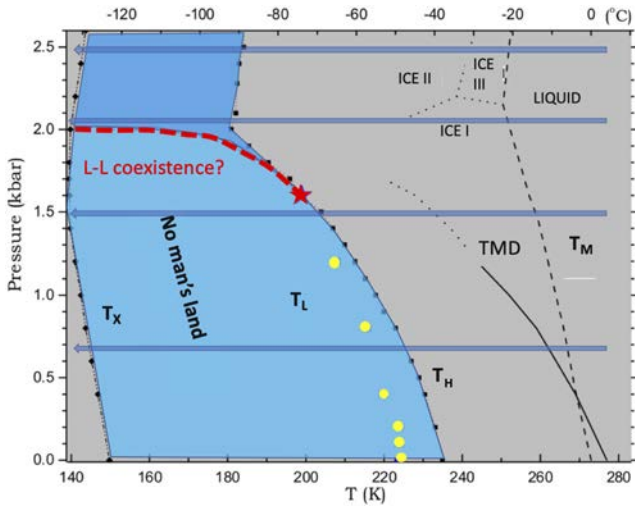


FIG. 1. Phase diagram of water, with superimposed Widom line data (T_L , yellow dots) for water confined in MCM-41 (figure redrawn from Ref. 16). The so-called *No man's land* is highlighted in blue: dark blue for the HDL region and light blue for the LDL region, separated by a red dashed line, corresponding to the liquid-liquid coexistence curve. The latter ends at the second critical point (red star). A Widom line (T_L) emanating from this point and represented by yellow dots has been drawn by Liu *et al.*¹⁶ T_H and T_X indicate the homogeneous nucleation temperature line and the crystallization temperature of amorphous solid water, respectively; TMD is the temperature of maximum density line, and T_M is the melting line. The P , T phase diagram for ices I, II, and III is also shown. The blue arrows indicate the isobaric paths investigated in the present work.

of water in different environments and under different thermodynamic conditions, allowing us to investigate the H-bonding interactions on length scales covering several orders of magnitude: from the molecular (local) scale to the mesoscopic scale typical of the Hydrogen Bond (HB) network. This can be achieved by combining the midinfrared (MIR) region ($1000 < \nu < 6000$ cm^{-1}) and the low-frequency domain known as the far-infrared (FIR) region ($\nu < 600$ cm^{-1}). MIR and FIR spectroscopies allow monitoring the evolution of both intramolecular and intermolecular vibrational modes of water, through the OH-stretching band (in the MIR range) and the so-called connectivity band arising from the collective dynamics of the HB network (in the FIR range). Needless to say, previous literature on this matter^{16,35–38} is controversial. Indeed, some authors interpret the changes in the IR spectral line shapes of confined liquid water when lowering the temperature as a signature of a structural change from a predominantly high-density liquid phase (HDL) to a lower-density phase (LDL) as the Widom line is crossed,^{16,36,37} conversely, other authors ascribe these changes to a liquid-solid phase transition.^{35,38} In particular, according to Liu and co-workers,¹⁶ upon lowering the temperature, T , at constant pressure, P , in the one-phase region, i.e., at $P < P_C$ (blue arrows in Fig. 1), one should observe a discontinuous change in the collective vibrational dynamics, corresponding to the cusplike FSC transition observed when crossing the so-called Widom line (yellow circles in Fig. 1). On the contrary, at $P > P_C$, when the L - L coexistence line is crossed, the sample would evolve from a predominantly HDL phase to a predominantly LDL one, passing in a continuous manner through mixtures of different proportions of HDL and LDL, and effects on the vibrational as well as on the relaxational dynamics should be washed out. Other authors^{29,30} interpret the dynamical crossover observed below P_C outside the scenario set by the crossing of the Widom line. On the other hand, it is not clear why crossing the L - L coexistence line should not induce a discontinuous change in the dynamics, if a phase transition between two liquid states takes place. As a consequence, we believe that a deeper investigation of the vibrational dynamics of water is on demand and report here new IR spectroscopy experiments on confined water, in order to test the scenario of Liu and co-workers¹⁶. Measurements have been performed in both MIR and FIR energy intervals. This approach allows us to study at the same time the variation of the molecular vibration strength due to the local environment modifications and the collective vibrational dynamics, which is sensitive to the relaxation dynamics of the system, respectively. The thermodynamic range investigated covers several isobars in the 0.7–3 kbar range and temperatures down to ~ 120 K.

We show that the observed changes in the OH-stretching band with temperature and pressure can be interpreted without invoking the crossing of a Widom line and that the MIR spectra suggest the nucleation of ice inside the confinement pores.

II. METHODS

A. Sample preparation

The experiment has been performed on water confined in a sample of MCM-41/C10 (pore size 2.8 nm and total pore volume 0.5 ml/g). Details on the synthesis procedure are described elsewhere.³⁹ The MCM-41/C10 powder has been hydrated by exposure to water vapor, to a level of hydration $h \sim 0.44$ g of H_2O /g of

dry MCM. This water content corresponds to a pore fillin slightly greater than 90% but still not too high to expect a significant amount of water pushed outside the pore volume on cooling at low pressure. In fact, the sample has been probed under pressure, and in such a case, a full pore fillin should be preferred in order to avoid a possible collapse of the porous matrix structure as the pressure is applied. The pore size has been chosen because no water freezing is claimed in MCM-41 with pore diameter ≤ 3 nm,^{27,40,41} and the reported suppression of crystallization allows us, in principle, to investigate supercooled water over a wide range of temperatures. However, it has to be mentioned that Johari and co-workers^{42,43} have observed an endothermic peak at ~ 220 K on heating, from 160 K, a sample of water in similar MCM materials with a pore size ~ 2.4 nm, ascribable to gradual melting of ice in the nanopores.

B. Infrared spectroscopy experiments

Infrared spectra have been collected at the AILES beamline (SOLEIL synchrotron, FR). All the spectra have been recorded in the transmission mode, by using a Bruker IFS 125 Fourier transform spectrometer (FT-IR), equipped with a bolometer detector (even though in the midinfrared region a MCT photodetector is often preferred), with a resolution of 2 cm^{-1} . 100 scans per spectrum have been recorded. In particular, the midinfrared region ($1000 < \nu < 6000\text{ cm}^{-1}$) has been investigated by means of a Globar lamp (internal source), in combination with a KBr beam splitter, whereas in order to obtain a sufficientl high signal-to-noise ratio, in the far-infrared region ($50 < \nu < 600\text{ cm}^{-1}$), we have used the infrared emission of the synchrotron radiation, with much higher brilliance with respect to a laboratory source. The synchrotron light was used in combination with a composite Si beam splitter. In order to control temperature and pressure, we have used a diamond anvil cell, namely, a Toullec membrane diamond anvil cell (MDAC) type, made of Inconel alloy, with $600\text{ }\mu\text{m}$ culet size and stainless steel gasket ($300\text{ }\mu\text{m}$ diameter \times $60\text{ }\mu\text{m}$ thickness), from Betsa.⁴⁴ This has been inserted in a helium closed circuit cryostat (pulse tube refrigerator cold head model CryoMec PT405) setup pumped down to a vacuum of $\sim 10^{-6}$ mbar, allowing to reach temperatures in the $4 < T < 300\text{ K}$ range. A thermocouple and a resistive heater have been used to control the sample temperature, which has been measured near the sample holder by using a silicon diode, with an accuracy on sample of about $\pm 0.1\text{ K}$.⁴⁵ Ruby was used as a pressure calibrant, and the pressure was determined based on the displacement of the R1 and R2 ruby fluorescence lines.⁴⁶ A small amount of hydrated powder sample has been loaded within the micrometer-sized hole between the diamonds. Then, a few drops of oil, used as pressure transmitting medium, and the ruby chips needed for pressure calibration have been added. In this context, the fundamental requirement for a pressure transmitting medium is its IR-transparency, i.e., absence of significant spectral features in the frequency domain of interest. Consequently, in the MIR region, we have used Fluorolube[®] as a transmitting medium. This is a saturated, hydrogen-free, low-molecular weight polymer of chlorotrifluoroethylen (CTFE), chemically inert under many demanding conditions. It is ideal for preparation of samples to be investigated from 4000 to 1360 cm^{-1} , where it exhibits only a very weak absorption band at $\sim 2300\text{ cm}^{-1}$, which is outside the frequency range of interest here. For the measurements in the far-infrared range, we have used instead nujol, a mineral

oil with high molecular weight. It is chemically inert, being essentially a heavy paraffin oil, i.e., a long chain alkane ($\text{C}_n\text{H}_{2n+2}$). Its IR spectrum shows major peaks at $2950\text{--}2800$, $1465\text{--}1450$, and $1380\text{--}1370\text{ cm}^{-1}$; thus, it is ideal for measurements below 1000 cm^{-1} . The efficiency of these pressure transmitting media within nanoporous matrices is discussed in Refs. 47 and 48. The cell environment was kept under vacuum ($\sim 10^{-5}$ to 10^{-6} mbar) for the duration of the entire experiment.

MIR spectra have been recorded at (0.7 ± 0.3) kbar, (1.5 ± 0.1) kbar, (2.00 ± 0.03) kbar, and (2.50 ± 0.06) kbar, while the FIR spectra were acquired at (1.1 ± 0.2) kbar, (1.6 ± 0.1) kbar, (2.1 ± 0.2) kbar, and (3.00 ± 0.01) kbar. At each pressure, the temperature ranged from 143 to 293 K, in steps of ~ 10 K. The pressure has been set at ambient temperature for each isobar and further checked after heating the sample at ambient temperature at the end of each temperature run. The pressure values reported above are average of the two measurements performed before and after each temperature run. Accordingly, their uncertainties are due to the observed pressure changes and are larger at the lower pressures, due to the higher instability of the DAC over cycling the temperature at relatively low pressures. For each pressure, IR spectra were acquired both on cooling and warming, in order to check for possible thermal hysteresis phenomena. In Fig. 2, the spectra obtained upon cooling and warming at some selected temperatures and $P = 1.1$ kbar over the FIR frequency domain are compared, as an example. Although some slight differences in intensity can be detected, due to unavoidable small changes in the alignment of the optical components, the spectral shape is essentially the same for close temperatures. For this reason, we report hereafter only the analysis performed on IR

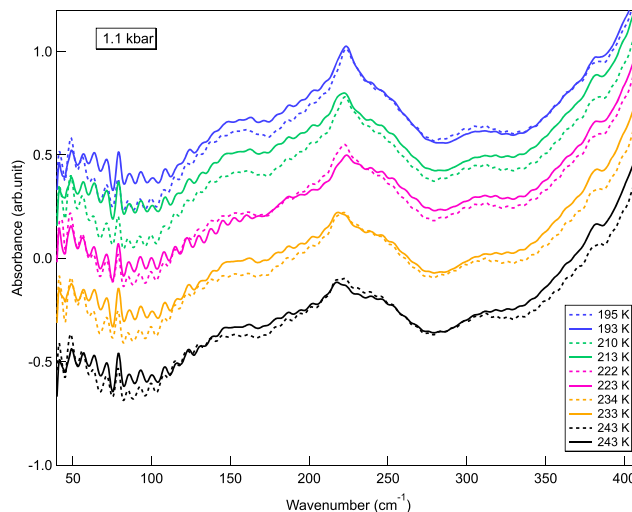


FIG. 2. Comparison between FIR spectra acquired along cooling (solid lines) and warming (dashed lines) paths for some selected temperatures at 1.1 kbar. The comparison is of the same quality at all investigated thermodynamic points, also in the case of MIR spectra. No signatures of thermal hysteresis occur as spectra are perfectly reproducible on cooling and warming. The small differences in intensity can be ascribed to unavoidable disalignment of the optical components throughout the experiment. Notice that here we show the raw data, prior to wavelet denoising, signal detrending, and polynomial background subtraction, as described in the text. Curves have been arbitrarily shifted along the vertical axis for clarity.

spectra recorded on cooling. Before collecting IR spectra of the hydrated sample, we have measured the spectra of the dry MCM-41/C10 matrix in order to verify that it does not show any relevant absorbance band in the spectral range of interest (data not shown).

The absorbance, A , of the sample is defined as

$$A = \log_{10} \left(\frac{I_0}{I_S} \right), \quad (1)$$

where I_S and I_0 are the transmitted intensity of the sample and the reference, respectively. In this experiment, for each sample, we have used as reference the DAC loaded only with the pressure transmitting medium.

C. Data reduction

IR absorption spectra were affected by large and nonperiodic oscillations superimposed to the signal embedding physical information. Such oscillations were likely ascribable to multiple reflections of the incident radiation beam bumping into the different interfaces inside the sample or bouncing around between the two windows of the sample container. Since attempts to clean up the raw signals by using conventional filtering methods (e.g., smoothing algorithms and Fourier filters) proved to be unsuccessful, we opted for the Stationary Wavelet Decomposition (SWT denoising 1D) technique. The latter was performed by adapting the MATLAB[®] dedicated toolbox to our purpose and allowed us to efficiently remove noise and all unwanted features from the IR spectra at all frequencies, overcoming the limits imposed by the most common and widely employed denoising techniques. A more detailed and in-depth description of the wavelet-based algorithm implemented is given in Ref. 49. Across each IR band deserving further analysis, wavelet denoising was followed by signal detrending, performed by using a home-made MATLAB[®] code, and polynomial background subtraction, computed by IGOR Pro[®] using the multiplex fitting package, in order to obtain a flat baseline. After the fulfillment of this three-step data reduction procedure, FIR spectra were ready for discussion, while MIR spectra were additionally analyzed in terms of Gaussian deconvolution, as described in Sec. III.

III. EXPERIMENTAL RESULTS

A. Midinfrared spectra

MIR spectra have been collected in the frequency range 2500–4300 cm^{-1} , which is dominated by the water OH stretching band. Four isobaric paths were followed: Fig. 3 displays spectra collected at $P = 0.7$ kbar and $P = 2.5$ kbar, as a representative of the whole investigated pressure range. All spectra show the same phenomenology observed in bulk water,⁵⁰ namely, they become sharper and their maxima move to smaller wavenumbers with lowering T . Differently to what found in bulk water, in all spectra, we notice a small feature at about 2600 cm^{-1} , whose origin is not clear. Excluding the presence in the substrate of left over hydrocarbon impurities from the surfactant, which are expected to contribute with a CH stretching band at ~ 2800 to 2900 cm^{-1} , previous literature suggests that this weak band is due to radiation-induced defects or to the mesoporous silica matrix structure.³⁵ In any case, this band is not associated with

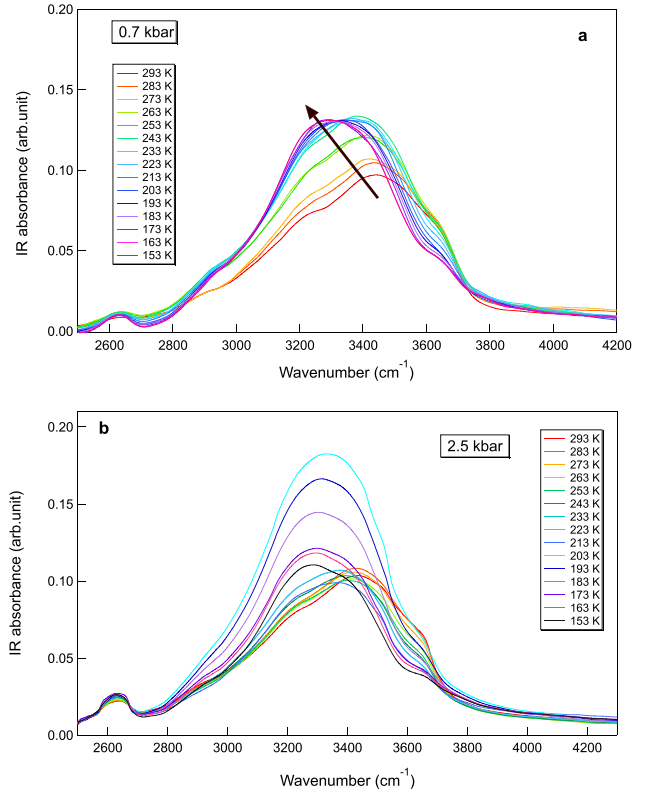


FIG. 3. MIR spectra in the OH stretching region at the lowest (a) and highest (b) pressure investigated, as a function of temperature. The arrow in panel (a) indicates the shift of the maximum of the band.

the spectrum of water and being temperature-independent has not been included in the spectral analysis of the OH-stretching band described in the following.

The observed shift of the OH stretching band can be better visualized in Fig. 4. Data at $P \leq 1.5$ kbar are in line with those of Zanotti *et al.*,³⁸ recorded at ambient pressure on water at the surface of the larger pores of Vycor glass. These authors observe two changes in slope in the temperature dependence of the position of the OH stretching band at ~ 160 K and 250 K [in agreement with Figs. 4(a) and 4(b)] and suggest that this is a signature of two dynamical transitions in the HB network. In the present case, the behavior of the band position vs T could be better described by a sigmoid, pointing out a continuous transition from a vibrational dynamics toward another. This transition becomes sharper at the two highest pressure states.

Better insight into the evolution of the intramolecular vibrational dynamics can be achieved by analyzing the behavior with temperature and pressure of the line shape of the OH stretching band. Under all conditions, in bulk or under confinement this band is very broad, with a line shape that cannot be accounted for by considering the contributions of the symmetric and antisymmetric vibrations, intermolecular vibrational coupling, and Fermi resonance.⁵¹ However, an agreed theoretical framework for its interpretation is not available although there is a wide consensus on the idea that

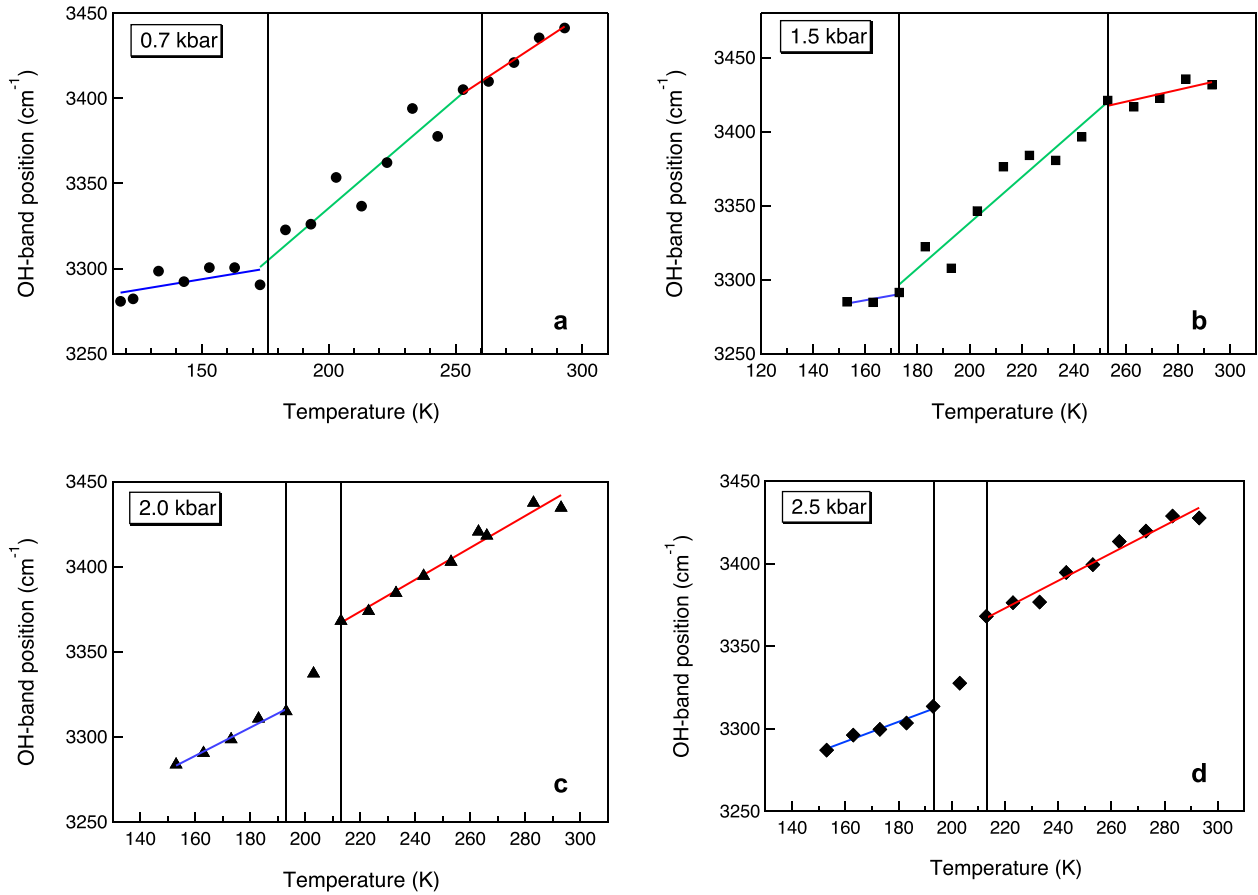


FIG. 4. Shift of the maximum of the OH stretching band with temperature at pressures $P = 0.7$ kbar (a), $P = 1.5$ kbar (b), $P = 2.0$ kbar (c), and $P = 2.5$ kbar (d). The vertical black lines are guides for the eyes, in order to highlight slope changes; the colored lines are best fits of the data.

the HB network of water and its modification must be responsible for its complex line shape and relevant intensity redistribution with changing thermodynamic conditions. As a consequence, the OH stretching band is usually fitted with four or five Gaussian lines, and questions regarding the vibrational dynamics of water are discussed in the light of the evolution of the Gaussian parameters with the thermodynamic state. A brief account of the different assignment of each individual Gaussian to a particular vibration or overtone, or to the stretching vibration of a particular kind of water molecules in the case of bulk water is reported in Ref. 52 and references therein. Here, we will compare our results with those of Ref. 36, where water confined in MCM-41 with the same pore dimensions of our sample was investigated. Following the criterion of minimizing the number of fit parameters, while preserving a good χ^2 , we have fitted our spectra by using four Gaussian lines (see Fig. 5), instead of five as done in Ref. 36.

We can assume that the width of the OH stretching band reflects the large number of different environments explored by the water molecules in the condensed phase. In this context, each Gaussian line reflects the vibrational dynamics of a different population of water molecules (molecules in different environments). Moreover, since the positions of the individual fitting Gaussian bands do not

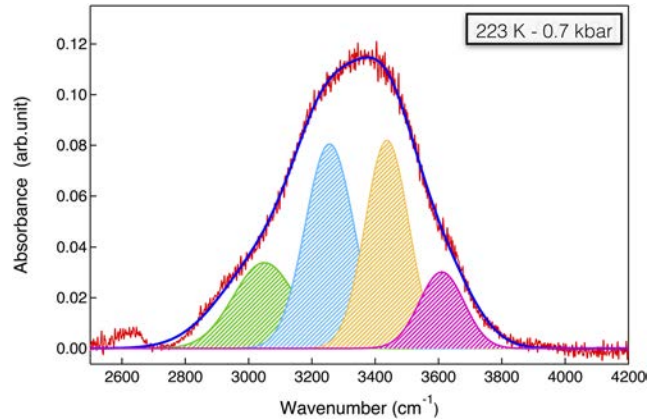


FIG. 5. Example of the spectral deconvolution of the OH-stretching band of confined water in the MIR frequency range, collected at 223 K and 0.7 kbar. For all temperatures, the OH-stretching band has been decomposed in four distinct intramolecular subbands modeled as Gaussian curves, centered around ~ 3080 cm^{-1} (green band, No. 1), ~ 3200 cm^{-1} (blue band, No. 2), ~ 3450 cm^{-1} (yellow band, No. 3), and ~ 3630 cm^{-1} (magenta band, No. 4). The red line represents the experimental data, whereas the overall fit is shown as solid blue curve.

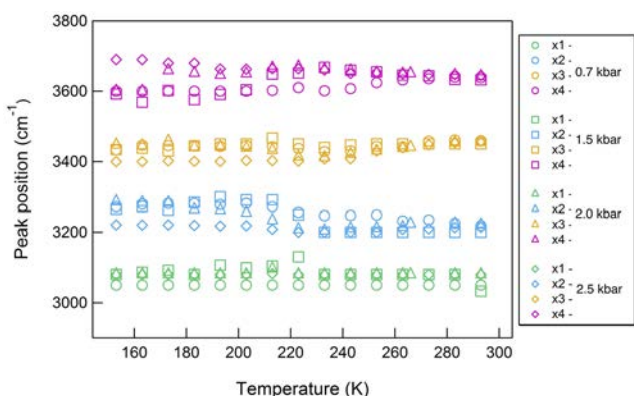


FIG. 6. Position, x_n with $n = 1, 2, 3, 4$, of the four Gaussian lines fitting the OH-stretching band of confined water as a function of temperature. Different colors refer to Gaussians 1, 2, 3, and 4 (according to the color code given in Fig. 5), and different symbols refer to different pressure states.

sensibly change with the thermodynamic parameters (see Fig. 6), we can argue that changes in their fractional intensity is symptomatic of changes in the relative populations of molecules experiencing different environments. The fractional intensity of each band is calculated as the integrated area under the single band relative to the total area of the spectrum. The temperature dependence of these intensities is reported in Fig. 7 at four pressure values.

Bearing in mind that the OH stretching band of isolated water molecules is centered at $\nu = 3656.65 \text{ cm}^{-1}$ ⁵² and that of ice is centered at $\nu = 3138 \text{ cm}^{-1}$,⁵³ we can assume that the components at the lowest (No. 1) and highest (No. 4) wavenumbers correspond to the populations of water molecules with the stronger and weaker H-bonds, respectively. As it clearly emerges from Fig. 7, the effect of temperature on such components is practically negligible. By considering that the error on the calculated fractional areas is around 20%, the fractional areas relative to components No. 1 and No. 4 can be regarded as constant over the investigated temperature range for all pressures. By contrast, the two dominant components (No. 2

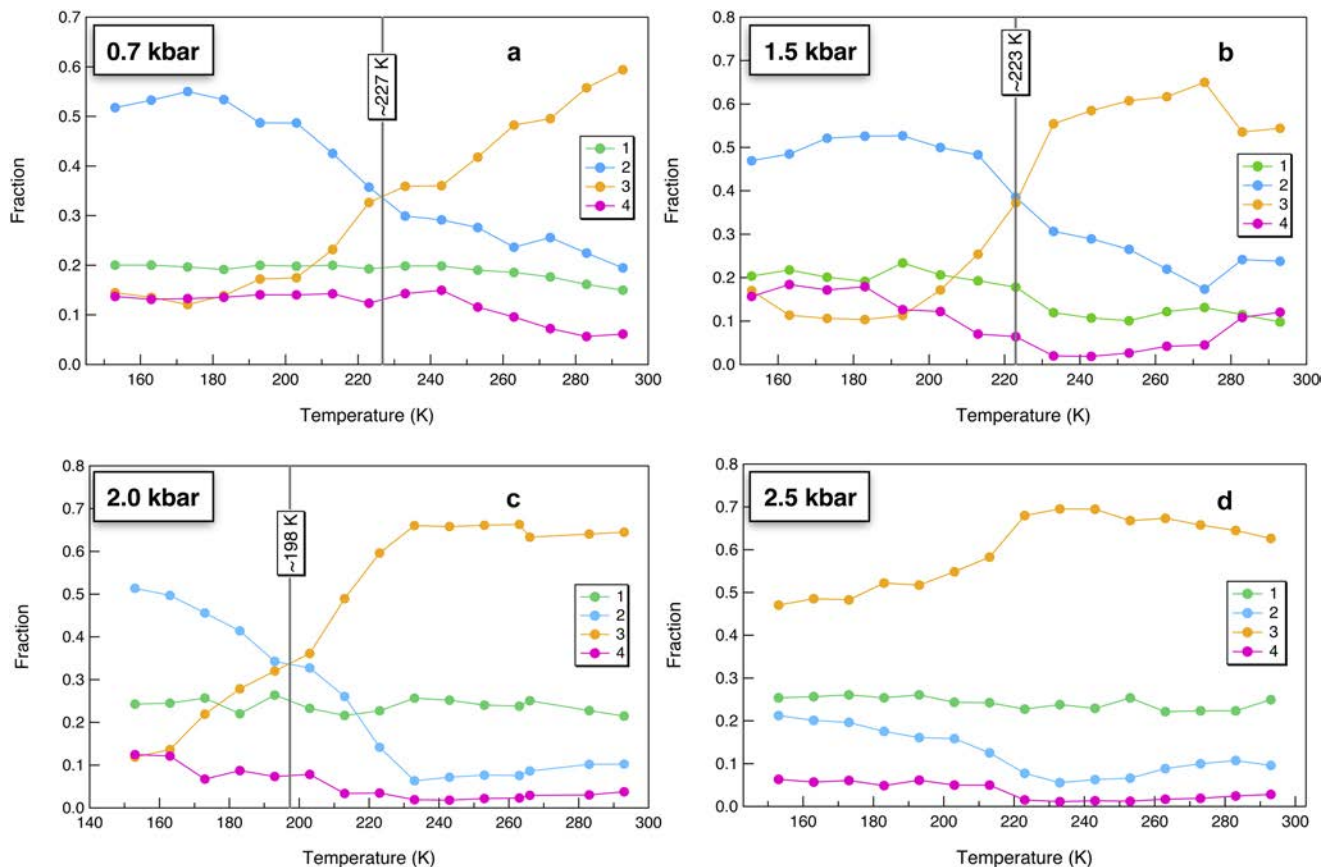


FIG. 7. Temperature evolution of the relative integrated areas of the spectral components contributing to the OH-stretching band of confined water along four isobaric paths, namely, 0.7 kbar in panel (a), 1.5 kbar in panel (b), 2.0 kbar in panel (c), and 2.5 kbar in panel (d). Each fractional area is labeled using the same number reported in Fig. 5 onto the single subbands. We remind that band No. 1 is ascribed to interfacial water; band No. 2 is ascribed to water molecules with a slow dynamics; band No. 3 is ascribed to water molecules with fast dynamics; and band No. 4 is ascribed to water molecules poorly engaged in the HB network. For pressures between 0.7 and 2.0 kbar, the vertical line indicates the temperature at which bands No. 2 and No. 3 cross each other.

and No. 3) appear to be heavily affected by temperature: their fractional areas follow opposite trends on decreasing temperature, varying between ~ 0.1 and ~ 0.6 . Moreover, a temperature can be identified at which the fractional areas relative to the two dominant subbands cross each other. This temperature decreases as the pressure increases. This behavior is verified for all pressures, except for the highest one (2.5 kbar), where the fractional intensity of band No. 2 stays always below 0.2, while that of band No. 3 exceeds 0.5 over the entire temperature range. Nevertheless, we notice a small intensity transfer between the two bands around 200 K. The above observations confirm that our data show the same phenomenology observed for confined water in Refs. 36 and 38 although the assignment of the individual components is debated. In particular, we propose the following assignments (for numbers and colors, we refer to Fig. 5):

- band No. 1 (green): interfacial water ($\nu \approx 3000\text{--}3100\text{ cm}^{-1}$).

It is well known that in confinement there is a non-freezable layer of water located at the pore wall interface, as discussed in Refs. 13, 24, 54, and 55. It is reasonable to hold that this interfacial water is less mobile than water inside the core pore, resulting in OH-bonds to oscillate with a lower frequency. Such an assignment agrees with recent findings reported in Ref. 38, where interfacial water shows

the OH-stretching band position at around 3100 cm^{-1} over the temperature range of our interest. The fraction of these water molecules is constant over the entire thermodynamic range investigated, in agreement with experiments^{8,55} and simulations.¹³

- band No. 2 (blue): water population with a slow dynamics ($\nu \approx 3150\text{--}3300\text{ cm}^{-1}$).

This band is usually assigned to water molecules with the highest degree of connectivity (coordination number close to 4), resulting in a strong H-bonding. Within the second critical point scenario, this component should dominate the absorbance profile of the low density amorphous (LDA) or LDL phase,³⁶ with structure and dynamics close to that of ice. Other authors, such as Venyaminov and Prendergast,⁵⁶ assign this band to the overtone of the bending ($2\nu_2$), enhanced by Fermi resonance.

- band No. 3 (yellow): water population with a faster dynamics ($\nu \approx 3350\text{--}3500\text{ cm}^{-1}$).

This band is usually assigned to the water component with an average degree of connectivity, implying less than four and weak H-bonds and a distorted H-bond network. Within the second critical point scenario, this component should dominate the absorbance profile of the high density amorphous (HDA) or HDL phase.³⁶ In the alternative

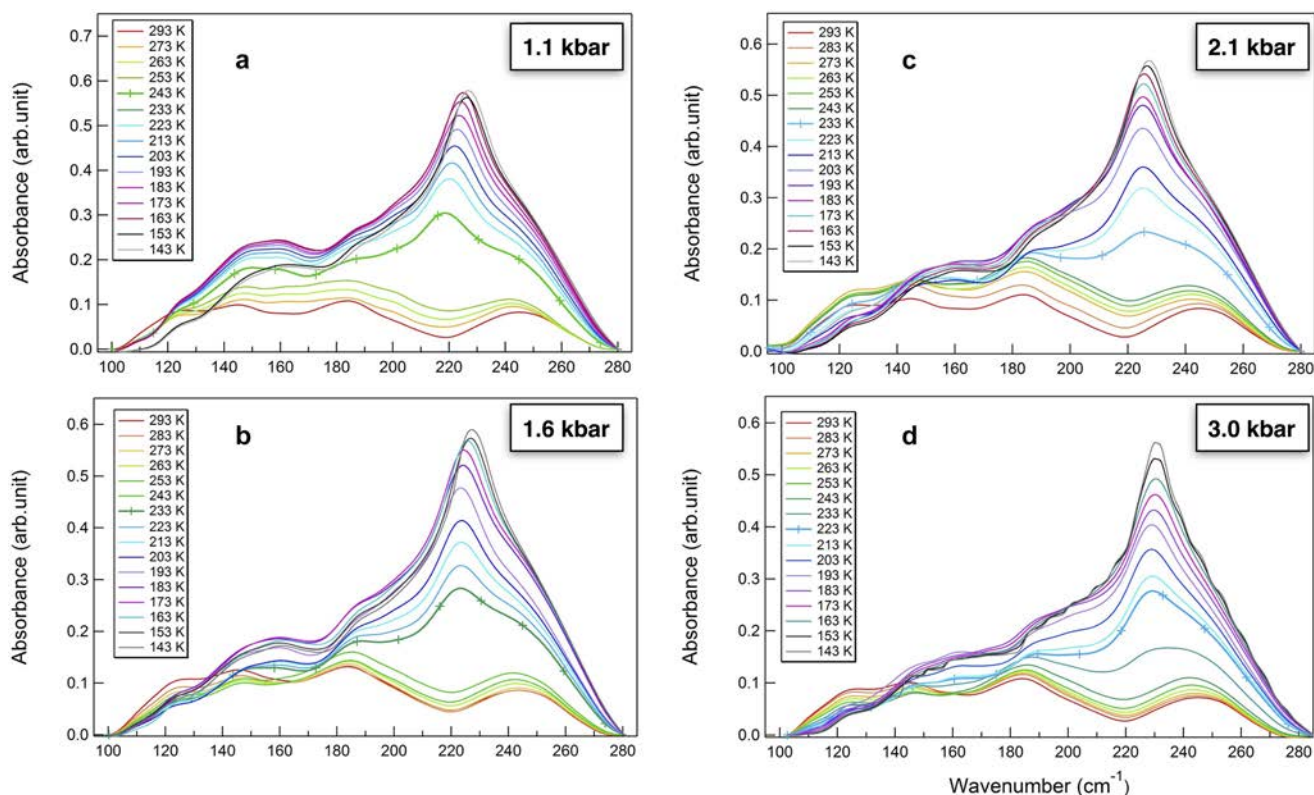


FIG. 8. Temperature evolution of the connectivity band of H_2O confined in MCM-41/C10 at different pressures [namely, 1.1 kbar in panel (a), 1.6 kbar in panel (b), 2.1 kbar in panel (c), and 3.0 kbar in panel (d)] after denoising and linear background subtraction described in Sec. II C. At each pressure, the temperature ranges from ambient down to 143 K, where water is deeply supercooled.

interpretation given in Ref. 56, this band corresponds to the symmetric stretching (ν_1).

- band No. 4 (magenta): water molecules not engaged in a HB network or poorly connected ($\nu \approx 3600\text{--}3650\text{ cm}^{-1}$). In the alternative interpretation given in Ref. 56, this band corresponds to the asymmetric stretching (ν_3). Also the intensity of this component is almost constant with temperature although it seems to decrease with increasing pressure.

According to Refs. 36 and 57, the intensity exchange between bands No. 2 and No. 3 and their crossing at a temperature between 198 K and 227 K below 2.5 kbar bring evidence for the crossing of a Widom line with negative slope (see the yellow points in Fig. 1), ending at the second critical point. The intensities of the two bands do not cross each other at the highest pressure state that is above the critical point. However, in our opinion, an alternative interpretation is possible. As a matter of fact, we do not see any sharp transition in all bands parameters: frequency, width, and relative intensity (see Figs. 4, 6, and 7). Thus, our data suggest that the OH-stretching dynamics of water confine in MCM-41 at pressures from ambient to 2 kbar continuously evolves with lowering the temperature from predominantly liquidlike (band No. 3) to predominantly ice-like (band No. 2) vibrations. At the highest pressure (2.5 kbar), the

intensity exchange is no more visible because at this pressure, the H-bonds are strongly distorted and icelike molecular configuration are not likely in the liquid. As a matter of fact, this is the pressure where the water structural, dynamical, and thermodynamic anomalies tend to disappear and the normal behavior is recovered.^{58,59}

B. Far-infrared spectra

Far-infrared spectra have been recorded at four pressure states between 1.1 kbar and 3.0 kbar at temperatures ranging from 293 K down to 143 K, in the ~ 0 to 400 cm^{-1} range, in order to explore the spectral range corresponding to the so-called *connectivity band* of confine water (~ 50 to 400 cm^{-1}). At odds with the OH-stretching band, which is due to *intramolecular* vibrational modes, the connectivity band reflect the *intermolecular* motion. It arises from the longitudinal motion of the hydrogen atoms along the hydrogen bond axis and depends more directly on the hydrogen bond network vibrations.

In principle, FIR experiments should make accessible also the librational band of water (hindered rotations) at ~ 400 to 900 cm^{-1} . This was not the case in the present experiment because the very weak librational band was hidden by a more intense spectral component due to the silica matrix. This appears as a steep rise originating

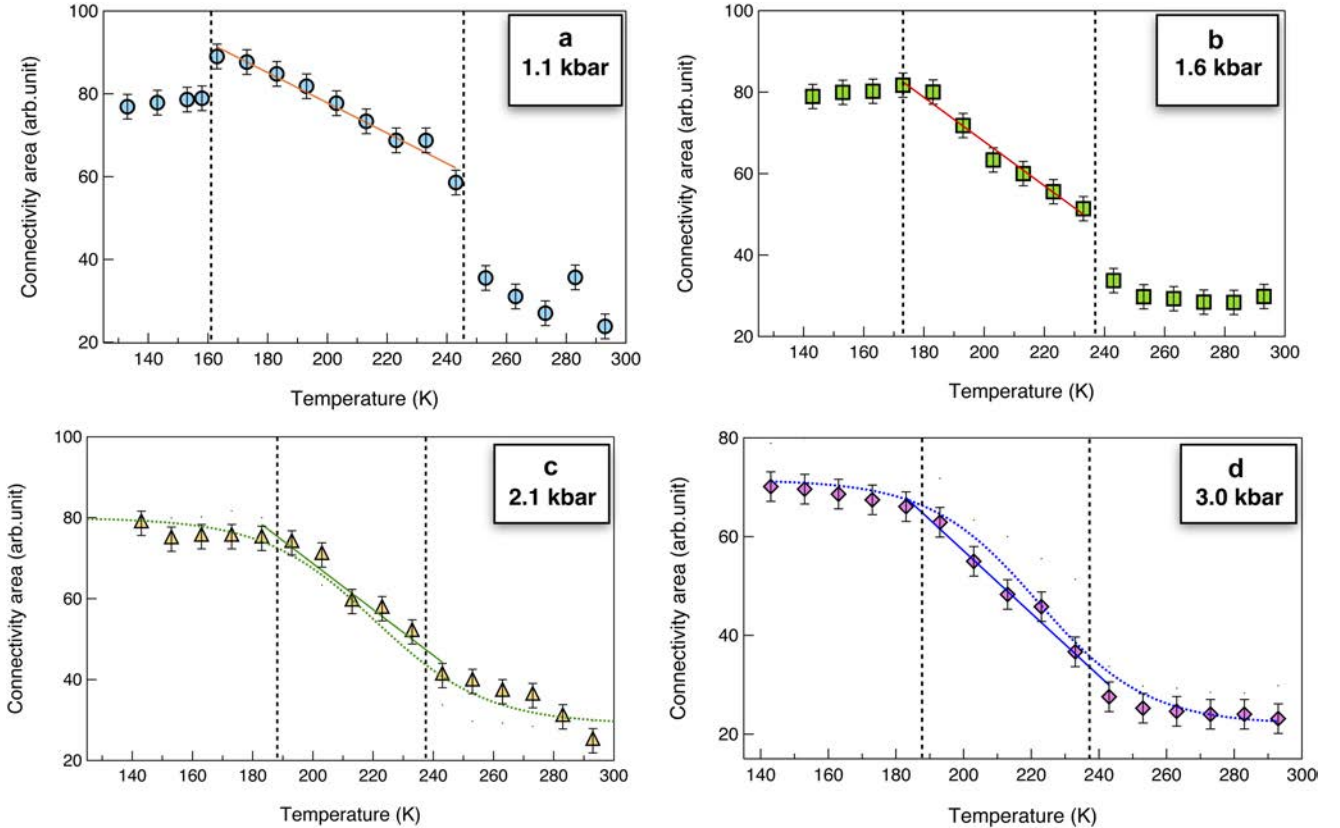


FIG. 9. Temperature evolution of the integrated area under the connectivity band (empty symbols) for each pressure, namely, 1.1 kbar in panel (a), 1.6 kbar in panel (b), 2.1 kbar in panel (c), and 3.0 kbar in panel (d). Solid lines are linear fits, while dotted curves are guides for the eyes. The vertical dotted lines evidence the temperatures at which dynamical transitions can be envisaged.

from $\sim 350\text{ cm}^{-1}$ upwards (Fig. 2). This rise has been subtracted as a background, during the preliminary data analysis described in Ref. 49 and Sec. II C.

Both the librational and connectivity bands are more sensitive probes of the hydrogen-bonding environment with respect to the OH-stretching band, as argued by studies of water confined within micelles.^{60,61} Thus, studies of water dynamics might particularly benefit from the information embedded in the low frequency region of the IR spectrum. Nevertheless, librational and connectivity bands remain under-represented in the literature due to the experimental difficulties in exploring the corresponding spectral ranges.

Our spectra, shown in Fig. 8, are in substantial agreement with previous literature on bulk and confined water,^{38,60} as far as the temperature evolution of their integrated intensity is concerned. In particular, Fig. 9 shows that the integrated area under the connectivity band increases by lowering the temperature. Moreover, at room temperature, the sample exhibits the FIR spectrum typical of bulk liquid water. This is characterized by a broad band with two or three bumps below $\sim 220\text{ cm}^{-1}$ plus a band at $\sim 240\text{ cm}^{-1}$. Initially, on entering the supercooled region, the line shape of the band does not substantially change, until an abrupt variation is observed at a temperature that is pressure dependent. As shown in Fig. 8, at each pressure, there is a temperature, T^* , at which an extra peak between 220 and 230 cm^{-1} shows up. This spectral contribution becomes more intense and sharper as the temperature is further reduced. The spectra recorded at T^* are highlighted by crosses in Fig. 8. If we assign each component of the FIR spectrum to molecules experiencing different HB strength and networking, as done for the MIR ones, then the appearance of an additional spectral contribution must be interpreted as an indication of the presence of a new population of water molecules at T^* . As a matter of fact, a comparison of our spectra with those of ice³⁸ unambiguously proves the nucleation of a solid phase inside the porous matrix.

The “transition” temperature, T^* , changes with pressure (243 K at 1.1 kbar, 233 K between 1.6 and 2.1 kbar, and 223 K at 3.0 kbar), consistently with a negative-slope of the liquid-solid coexistence line in the P - T phase diagram of water. The transition from a fully liquid system to a liquid-solid coexistence becomes less sharp as the pressure increases.

IV. DISCUSSION

It has been established that the vibrational modes involving the intramolecular OH-stretching are sensitive to the strength of the H-bonding between water molecules.⁶⁰ As a result, the OH-stretching band, probed in the MIR range, has a very complex structure as it spans a broad frequency range corresponding to manifold dynamic regimes. As shown for liquid water below its melting point, the broad band observed in the MIR region has to be regarded as a continuous distribution of H-bond frequencies, not necessarily due only to stretching but possibly linked to other vibrational modes.⁶² From this point of view, a description of the OH-stretching band in terms of multicomponent models is far to be trustworthy and unambiguously correlated with the real structure and dynamical behavior of the system.⁶³ In addition, it has been recently pinpointed that, unlike many other simpler liquids, H_2O is characterized by a strong coupling between its vibrational modes and by a nonadiabatic vibrational dynamics.⁶⁴ This implies that stretching,

bending, and intermolecular modes cannot be treated as independently evolving, but their strongly mixed character needs to be taken into account as IR spectra are analyzed. That is to say, it is not possible to correctly describe the OH-stretching vibration of water simply as a local bond stretching or as the linear combination of symmetric/asymmetric modes; it is rather to be regarded as the result of a collective and complex excitation of a cluster made up by several molecules.^{52,65} For this reason, we interpret the results of the MIR spectra at the light of what is seen in the FIR region. Consequently, attempting to establish a direct link between the Gaussian subbands and the number of H-bonds formed by water molecules seems to be a quite oversimplified description, which might lead to a misleading interpretation of the information brought by the MIR spectra. Conversely, each substructure of the spectrum is representative of a water population with a distinct dynamic behavior.

Making reference to the assignments done in Sec. III A, we notice that components No. 2, 3, and 4 correspond to the components identified in the MIR spectra of both bulk and confined water investigated by other authors^{36,60} although a different interpretation has been proposed. Conversely, component No. 1, which in our picture reflects the behavior of pore interfacial water, cannot be identified in bulk water. It is also absent in the deconvolution strategy adopted by Ref. 36 for the decomposition of MIR spectra relative to confined water. Although a similar counterpart has not been identified in previous literature, this component was necessary to obtain a satisfactory deconvolution of our MIR spectra at all temperatures and pressures. Moreover, its presence is fully consistent with the proposed interpretation and independent evidences from MD simulations¹³ and experiments.^{8,9,55}

A useful overall view of the information that can be extracted from MIR spectra is given by the fractional area calculated for each component as a function of temperature at fixed pressure (Fig. 7). Indeed, at all pressures, the fraction of interfacial water molecules (green) settles at $\sim 20\%$ and is almost independent of temperature, with a slight increase at higher pressures. These latter water molecules, being dynamically “arrested,” cannot experience a temperature-driven transition from a disordered phase (liquid or glassy) to a more ordered one (ice). Also the population of isolated (not-networking) water molecules is quite small (less than 20%), with a temperature behavior closely resembling that of interfacial water. What is more interesting is the interplay between the two water populations contributing in the middle of the OH-band and their evolution with temperature. In particular, while the fraction of “slower” water molecules continuously increases as the temperature decreases, the fraction of “faster” water molecules undergoes the opposite trend. By observing Fig. 7, it clearly emerges that the “slower” (predominantly liquidlike) and “faster” (predominantly solidlike) water populations swap their roles at a given temperature. Indeed, starting from room temperature, water inside the core pore is mostly represented by molecules with a “faster” dynamics. This holds true also in the supercooled regime until a transition temperature is reached. Such a temperature signs an inflection point (crossover); as the temperature is lowered further, the “slower” population becomes dominant. For pressures higher than 2.0 kbar, the inflection point disappears. This means that water above 2.0 kbar dynamically behaves as a more homogeneous system, whose composition in terms of slow/fast components does not change noticeably with temperature. Apparently, the dynamical behavior of water

becomes less sensitive to the temperature at $P \sim 2.5$ kbar and above it. Indeed, although the temperature is lowered by more than 100 K, the water populations identified by components Nos. 2 and 3 do not dramatically change and the “faster” component is dominant over the whole temperature range. This probably happens because high pressures hinder the formation of regular and extended clusters of hydrogen-bonded water molecules. As a matter of fact, here we are at the border of ice III formation (see Fig. 1), which has a totally different topology with respect to ice Ih. It contains five-membered rings and has the lowest density among the high pressure ice forms, very similar to the density of liquid water at the same pressure. As a consequence, the HBs are more distorted; thus, the system is overall less rigid and the “slower” population gives only a little contribution. We conjecture that this behavior may be connected to the anomalous pressure dependence of the self-diffusion coefficient^{58,66,67} and viscosity⁶⁸ of supercooled bulk water. These quantities show a maximum or a minimum, respectively, between 1.5 and 2.0 kbar, at about the same pressure at which water molecules approach their first neighbors more closely.⁶⁹ The maximum of the self-diffusion coefficient (minimum of viscosity) vs P is consistent with the dominance of the “faster” water population above 2.0 kbar as pointed out in our experiments.

Since a link between the local structure of water and its dynamics is expected,⁷⁰⁻⁷² some authors⁷³ have suggested the possibility that large changes in intramolecular vibrational properties may be connected to the onset of fractional Stokes-Einstein (SE) behavior.^{14,74,75} Figure 7 seems to confirm the presence of a coexistence line in the water phase diagram, in agreement with Ref. 76 and apparently supports the results provided by other studies^{36,57} on water confined in MCM-41-S15 using Raman and FTIR spectroscopy. Nevertheless, our interpretation departs from this picture and is supported by the combination of MIR data with previous analysis of neutron diffraction experiments,⁵⁵ with the present FIR data, and with previous evidence that deviations of the diffusion coefficient of water from the Stokes-Einstein equation are not necessarily due to the crossing of a transition line.⁷⁷

As a matter of fact, we have seen a new band showing up in the FIR spectra. At each pressure, this occurs at a temperature very close to the temperature of crossover of spectral components Nos. 2 and 3 of the MIR spectra. Thus, the two findings must be correlated. In particular, the crossover of bands Nos. 2 and 3 has been interpreted as due to a predominantly icelike dynamics at the lower temperatures; accordingly, the appearance of the new band in the FIR spectra can be regarded as the signature of the formation of a solid phase within the pore volume. This statement can be easily confirmed by comparing our experimental FIR spectra with the signal of hexagonal ice, amorphous ice, and liquid water reported in Fig. 2 of Ref. 38 over the same frequency range. At ambient temperature, the connectivity band is typical of liquid water and preserves the same characteristics down to 253 K. By cooling the system further, a well-defined peak arises at 220 cm^{-1} and progressively shifts between 220 and 230 cm^{-1} , closely resembling the peak assigned to crystalline ice.³⁸ This implies that a transition temperature can be identified between 253 and 243 K: starting from ambient temperature, water confined in the porous silica substrate is originally liquid, and then, the onset of a solid phase leads to the coexistence of ice and supercooled liquid water within the pore. As long as the temperature is lowered, the solid phase nucleates and the

intensity profile looks like that expected for crystalline ice (Fig. 2 of Ref. 38).

V. CONCLUSIONS

We have shown that the P-T behavior of FIR and MIR spectra of water confined in MCM-41 can be easily interpreted in terms of a liquid-solid transition, taking place in correspondence of a coexistence line with negative slope, without invoking the existence of a Widom line or second critical point. We stress that this is possible only if the both frequency ranges are recorded for the same sample and interpreted as a whole. As a matter of fact, while the MIR spectra may be interpreted also in terms of a transition from LDL to HDL, as done in Ref. 36, the FIR spectra clearly discriminate between the two scenarios. Indeed, the temperature and pressure evolution of the MIR spectra proves the coexistence of two dominant water populations inside the pore volume; nevertheless, this is not sufficient to unambiguously confirm that two kinds of liquids differing in density exist in the supercooled region of the water phase diagram. As a matter of fact, FIR data clearly point out the nucleation of a solid phase in the pore core, in agreement with accurate differential scanning calorimetry.^{42,43} This excludes the coexistence of two liquid forms in water confined in MCM-41, in favor of a liquid-solid transition of at least a fraction of the water molecules as the temperature is lowered below 240–250 K. The present interpretation of the P-T evolution of the vibrational dynamics of water confined in MCM-41 is in agreement with the results of a neutron diffraction experiment performed on the same sample at ambient pressure.⁵⁵ Indeed, also in that experiment, it has been seen that a non-negligible fraction of water confined in MCM-41/C10 (pore diameter 2.8 nm) crystallizes at 240 K as a stacking fault ice I at the center of the pore. This fraction coexists with about one or two layers of nonfreezable water at the pore wall.

Summarizing, we want to highlight that often a single experimental technique, or investigation of a limited dynamical range, is not enough in order to draw unambiguous conclusions. We are instead confident about our interpretation of the IR spectra of water as this has been based on the study of a wide spectral range and having in mind the structural information extracted from neutron diffraction experiments.⁵⁵ Finally, we want to mention that a correct interpretation of any experimental data cannot disregard the accuracy and sensitivity of the experimental technique. As a matter of fact, the claim of the absence of crystallization in severe confinement^{27,40,41} and of a fragile to strong crossover¹⁶ may likely be due to experimental limits of the instruments or technique.

REFERENCES

- 1 J. Dore, *Chem. Phys.* **258**, 327 (2000).
- 2 M.-C. Bellissent-Funel, *J. Mol. Liq.* **84**, 39 (2000).
- 3 C. E. Bertrand, Y. Zhang, and S.-H. Chen, *Phys. Chem. Chem. Phys.* **15**, 721 (2013).
- 4 R. K. Hawkins and P. A. Egelstaff, *Clays Clay Miner.* **28**, 19 (1980).
- 5 N. Giovambattista, P. G. Debenedetti, and P. J. Rossky, *J. Phys. Chem. B* **111**, 9581 (2007).
- 6 N. Giovambattista, P. G. Debenedetti, and P. J. Rossky, *J. Phys. Chem. C* **111**, 1323 (2007).
- 7 L. Hua, X. Huang, P. Liu, R. Zhou, and B. J. Berne, *J. Phys. Chem. B* **111**, 9069 (2007).

- ⁸R. Mancinelli, S. Imberti, A. K. Soper, K. H. Liu, C. Y. Mou, F. Bruni, and M. A. Ricci, *J. Phys. Chem. B* **113**, 16169 (2009).
- ⁹R. Mancinelli, F. Bruni, and M. A. Ricci, *J. Phys. Chem. Lett.* **1**, 1277 (2010).
- ¹⁰I. M. Briman, D. Rebiscol, O. Diat, J.-M. Zanotti, P. Jollivet, P. Barbour, and S. Gin, *J. Phys. Chem. C* **116**, 7021 (2012).
- ¹¹N. C. Osti, A. Coté, E. Mamontov, A. Ramirez-Cuesta, D. J. Wesolowski, and S. O. Diallo, *Chem. Phys.* **465**, 1 (2016).
- ¹²Y.-K. Cheng and P. J. Rossky, *Nature* **392**, 696 (1998).
- ¹³P. Gallo, M. Rovere, and S.-H. Chen, *J. Phys. Chem. Lett.* **1**, 729 (2010).
- ¹⁴H. Stanley, S. Buldyrev, G. Franzese, P. Kumar, F. Mallamace, M. G. Mazza, K. Stokely, and L. Xu, *J. Phys.: Condens. Matter* **22**, 284101 (2010).
- ¹⁵F. G. Alabarse, J. Haines, O. Cambon, C. Levelut, D. Bourgogne, A. Haidoux, D. Granier, and B. Coasne, *Phys. Rev. Lett.* **109**, 035701 (2012).
- ¹⁶L. Liu, S.-H. Chen, A. Faraone, C.-W. Yen, and C.-Y. Mou, *Phys. Rev. Lett.* **95**, 117802 (2005).
- ¹⁷O. Mishima and H. E. Stanley, *Nature* **392**, 164 (1998).
- ¹⁸R. Speedy and C. Angell, *J. Chem. Phys.* **65**, 851 (1976).
- ¹⁹S. Sastry, P. G. Debenedetti, F. Sciortino, and H. E. Stanley, *Phys. Rev. E* **53**, 6144 (1996).
- ²⁰P. H. Poole, F. Sciortino, T. Grande, H. E. Stanley, and C. A. Angell, *Phys. Rev. Lett.* **73**, 1632 (1994).
- ²¹F. Sciortino, P. H. Poole, U. Essmann, and H. E. Stanley, *Phys. Rev. E* **55**, 727 (1997).
- ²²J. L. F. Abascal and C. Vega, *J. Chem. Phys.* **133**, 234502 (2010).
- ²³J. C. Palmer, A. Haji-Akbari, R. S. Singh, F. Martelli, R. Car, A. Z. Panagiotopoulos, and P. G. Debenedetti, *J. Chem. Phys.* **148**, 137101 (2018).
- ²⁴D. T. Limmer and D. Chandler, *J. Chem. Phys.* **138**, 214504 (2013).
- ²⁵J. C. Palmer, P. H. Poole, F. Sciortino, and P. G. Debenedetti, *Chem. Rev.* **118**, 9129 (2018).
- ²⁶J. Teixeira, J.-M. Zanotti, M.-C. Bellissent-Funel, and S.-H. Chen, in *Proceedings of the First European Conference on Neutron Scattering* [Physica B **234-236**, 370 (1997)].
- ²⁷G. H. Findenegg, S. Jähnert, D. Akcakayiran, and A. Schreiber, *ChemPhysChem* **9**, 2651 (2008).
- ²⁸K. H. Kim, A. Späh, H. Pathak, F. Perakis, D. Mariedahl, K. Amann-Winkel, J. A. Sellberg, J. H. Lee, S. Kim, J. Park, K. H. Nam, T. Katayama, and A. Nilsson, *Science* **358**, 1589 (2017).
- ²⁹S. Cerveny, J. Colmenero, and A. Alegría, *Phys. Rev. Lett.* **97**, 189802 (2006).
- ³⁰J. Swenson, *Phys. Rev. Lett.* **97**, 189801 (2006).
- ³¹S.-H. Chen, L. Liu, and A. Faraone, *Phys. Rev. Lett.* **97**, 189803 (2006).
- ³²A. K. Soper, *Proc. Natl. Acad. Sci. U. S. A.* **108**, E1192 (2011), author reply E11934.
- ³³F. Caupin, V. Holten, C. Qiu, E. Guillermin, M. Wilke, M. Frenz, J. Teixeira, and A. K. Soper, *Science* **360**, eaat1634 (2018).
- ³⁴K. H. Kim, A. Späh, H. Pathak, F. Perakis, D. Mariedahl, K. Amann-Winkel, J. A. Sellberg, J. H. Lee, S. Kim, J. Park, K. H. Nam, T. Katayama, and A. Nilsson, *Science* **360**, eaat1729 (2018).
- ³⁵M. Erko, G. Findenegg, N. Cade, A. Michette, and O. Paris, *Phys. Rev. B* **84**, 104205 (2011).
- ³⁶F. Mallamace, M. Broccio, C. Corsaro, A. Faraone, D. Majolino, V. Venuti, L. Liu, C.-Y. Mou, and S.-H. Chen, *Proc. Natl. Acad. Sci. U. S. A.* **104**, 424 (2007).
- ³⁷W. A. Kamitakahara, A. Faraone, K.-H. Liu, and C.-Y. Mou, *J. Phys.: Condens. Matter* **24**, 064106 (2012).
- ³⁸J.-M. Zanotti, P. Judeinstein, S. Dalla-Bernardina, G. Creff, J.-B. Brubach, P. Roy, M. Bonetti, J. Ollivier, D. Sakellariou, and M.-C. Bellissent-Funel, *Sci. Rep.* **6**, 25938 (2016).
- ³⁹G. Lelong, S. Bhattacharyya, S. Kline, T. Cacciaguerra, M. A. Gonzalez, and M.-L. Saboungi, *J. Phys. Chem. C* **112**, 10674 (2008).
- ⁴⁰L. Liu, S.-H. Chen, A. Faraone, C.-W. Yen, C.-Y. Mou, A. I. Kolesnikov, E. Mamontov, and J. Leao, *J. Phys.: Condens. Matter* **18**, S2261 (2006).
- ⁴¹S. Jähnert, F. V. Chávez, G. Schaumann, A. Schreiber, M. Schönhoff, and G. Findenegg, *Phys. Chem. Chem. Phys.* **10**, 6039 (2008).
- ⁴²E. Tombari, G. Salvetti, and G. P. Johari, *J. Phys. Chem. C* **116**, 2702 (2012).
- ⁴³E. Tombari and G. P. Johari, *J. Chem. Phys.* **139**, 064507 (2013).
- ⁴⁴A. Voute, M. Deutsch, A. Kalinko, F. Alabarse, J.-B. Brubach, F. Capitani, M. Chapuis, V. T. Phuoc, R. Sopracase, and P. Roy, *Vib. Spectrosc.* **86**, 17 (2016).
- ⁴⁵S. Dalla Bernardina, F. Alabarse, A. Kalinko, P. Roy, M. Chapuis, N. Vita, R. Hienerwadel, C. Berthomieu, P. Judeinstein, J.-M. Zanotti, J. Bantignies, J. Haines, J. Catafesta, G. Creff, L. Manceron, and J.-B. Brubach, *Vib. Spectrosc.* **75**, 154 (2014).
- ⁴⁶H. K. Mao, J. Xu, and P. M. Bell, *J. Geophys. Res.: Solid Earth* **91**, 4673, <https://doi.org/10.1029/jb091ib05p04673> (1986).
- ⁴⁷S. C. McKellar and S. A. Moggach, *Acta Crystallogr., Sect. B* **71**, 587 (2015).
- ⁴⁸J. Im, N. Yim, J. Kim, T. Vogt, and Y. Lee, *J. Am. Chem. Soc.* **138**, 11477 (2016).
- ⁴⁹E. Stefanutti and F. Bruni, in *IMEKO TC19 Workshop on Metrology for the Sea, MetroSea 2017: Learning to Measure Sea Health Parameters* (IMEKO, 2017), Vol. 2017, pp. 104–110.
- ⁵⁰D. Klug and E. Whalley, *J. Chem. Phys.* **81**, 1220 (1984).
- ⁵¹Q. Hu, H. Zhao, and S. Ouyang, *Phys. Chem. Chem. Phys.* **19**, 21540 (2017).
- ⁵²M. Sbroscia, A. Sodo, F. Bruni, T. Corridoni, and M. A. Ricci, *J. Phys. Chem. B* **122**, 4077 (2018).
- ⁵³I. Auriakovia, R. Claverie, P. Bourson, M. Marchetti, J.-M. Chassot, and M. D. Fontana, *J. Raman Spectrosc.* **42**, 1408 (2011).
- ⁵⁴K. Morishige and K. Kawano, *J. Chem. Phys.* **110**, 4867 (1999).
- ⁵⁵E. Stefanutti, L. E. Bove, G. Lelong, M. A. Ricci, A. K. Soper, and F. Bruni, *Phys. Chem. Chem. Phys.* **21**, 4931 (2019).
- ⁵⁶S. Y. Venyaminov and F. G. Prendergast, *Anal. Biochem.* **248**, 234 (1997).
- ⁵⁷F. Mallamace, C. Branca, M. Broccio, C. Corsaro, C.-Y. Mou, and S.-H. Chen, *Proc. Natl. Acad. Sci. U. S. A.* **104**, 18387 (2007).
- ⁵⁸K. R. Harris and P. J. Newitt, *J. Chem. Eng. Data* **42**, 346 (1997).
- ⁵⁹J. R. Errington and P. G. Debenedetti, *Nature* **409**, 318 (2001).
- ⁶⁰J.-B. Brubach, A. Mermet, A. Filabozzi, A. Gerschel, and P. Roy, *J. Chem. Phys.* **122**, 184509 (2005).
- ⁶¹D. S. Venables, K. Huang, and C. A. Schmuttenmaer, *J. Phys. Chem. B* **105**, 9132 (2001).
- ⁶²Y. Maréchal, *J. Mol. Struct.* **1004**, 146 (2011).
- ⁶³J. D. Smith, C. D. Cappa, K. R. Wilson, R. C. Cohen, P. L. Geissler, and R. J. Saykally, *Proc. Natl. Acad. Sci. U. S. A.* **102**, 14171 (2005).
- ⁶⁴K. Ramasesha, L. De Marco, A. Mandal, and A. Tokmakoff, *Nat. Chem.* **5**, 935 (2013).
- ⁶⁵A. Paarmann, T. Hayashi, S. Mukamel, and R. J. D. Miller, *J. Chem. Phys.* **130**, 204110 (2009).
- ⁶⁶S.-H. Chen and P. Tartaglia, *Scattering Methods in Complex Fluids* (Cambridge University Press, 2015).
- ⁶⁷F. Bruni, A. Giuliani, J. Mayers, and M. Ricci, *J. Phys. Chem. Lett.* **3**, 2594 (2012).
- ⁶⁸L. P. Singh, B. Issenmann, and F. Caupin, *Proc. Natl. Acad. Sci. U. S. A.* **114**, 4312 (2017).
- ⁶⁹A. Okhulkov, Y. N. Demianets, and Y. E. Gorbaty, *J. Chem. Phys.* **100**, 1578 (1994).
- ⁷⁰M. G. Mazza, N. Giovambattista, F. W. Starr, and H. E. Stanley, *Phys. Rev. Lett.* **96**, 057803 (2006).
- ⁷¹N. Giovambattista, F. W. Starr, F. Sciortino, S. V. Buldyrev, and H. E. Stanley, *Phys. Rev. E* **65**, 041502 (2002).
- ⁷²F. Sciortino, P. H. Poole, H. E. Stanley, and S. Havlin, *Phys. Rev. Lett.* **64**, 1686 (1990).
- ⁷³L. Xu, F. Mallamace, Z. Yan, F. W. Starr, S. V. Buldyrev, and H. E. Stanley, *Nat. Phys.* **5**, 565 (2009).
- ⁷⁴S.-H. Chen, F. Mallamace, C.-Y. Mou, M. Broccio, C. Corsaro, A. Faraone, and L. Liu, *Proc. Natl. Acad. Sci. U. S. A.* **103**, 12974 (2006).
- ⁷⁵A. Dehaoui, B. Issenmann, and F. Caupin, *Proc. Natl. Acad. Sci. U. S. A.* **112**, 12020 (2015).
- ⁷⁶S.-H. Chen, Z. Wang, A. I. Kolesnikov, Y. Zhang, K.-H. Liu, M. Tokuyama, and I. Oppenheim, *AIP Conf. Proc.* **1518**, 77–85 (2013).
- ⁷⁷L. E. Bove, S. Klotz, T. Strässle, M. Koza, J. Teixeira, and A. M. Saitta, *Phys. Rev. Lett.* **111**, 185901 (2013).